



Nonlinear modelling and control of the flow over aerofoils using CFD simulations



H.D. Karaca^a, G.D. Özen^b, C. Kasnakoğlu^{a,*}

^a Department of Electrical and Electronics Engineering, TOBB University of Economics and Technology, Ankara, Turkey

^b Department of Physics, Middle East Technical University, Ankara, Turkey

ARTICLE INFO

Article history:

Received 8 March 2016

Revised 16 June 2016

Accepted 19 June 2016

Available online 1 July 2016

Keywords:

Flow control

Nonlinear dynamical modelling

Drag to lift control

Hammerstein–Wiener model

ABSTRACT

A simulation based approach for nonlinear dynamical modelling and feedback control of the drag to lift ratio for aerofoils is investigated through case studies involving NACA 23012, ag13 and b737a aerofoils. The flow around the aerofoils is studied via numerical solutions of the 2D Navier–Stokes (NS) equations. A standard computational fluid dynamics (CFD) solver is extended to be able to measure desired feedback values and to apply a control input to the flow field. The proposed modelling and control approach is based on first determining the measurement points and injection points on the aerofoil for the control input. Then, to estimate the dynamical model, some input–output data are collected by injecting a chirp input flow to the field and saving the measurement data. Next a Hammerstein–Wiener (HW) type nonlinear dynamical model of the flow field is estimated using system identification. For control design, the nonlinear part of the model is eliminated by means of inverse functions, followed by the application of automated tuning methods to the linear part to obtain the closed-loop system. The results show that the designed feedback control system can reduce the drag to lift ratio considerably as compared to the unactuated case.

© 2016 Elsevier B.V. All rights reserved.

1. Introduction

While an accurate mathematical representation of fluid flows can be achieved using the Navier–Stokes (NS) partial differential equations, these are very difficult to analyse due to their complexity and most of the time obtaining an analytical solution is impossible [1]. As a result, flow systems are typically studied numerically using computational fluid dynamics (CFD) methods; examples include bluff body flows [2], forced convection heat transfer [3] and non-Newtonian flows [4].

Flow control strategies have been investigated for many years to manipulate fluid flow and change its behaviour to control relevant variables such as vorticity, lift, drag, transition, separation and so on [5]. Analysing the fluid flow around aerofoils is one of the important problems in fluid mechanics. One sample problem of interest is to control the separation on aerofoils, which is the breakaway or detachment of fluid from a solid surface. Studies about this topic include Liang et al. [6] who used two types of plasma aerodynamic actuation excited by microsecond discharge and nanosecond discharge and Greenblatt and Wygnanski [7] who proposed an experimental method of periodic hydrodynamic excitation to control the separation. Another significant problem is the analysis and manipulation of the lift and drag forces which are formed due to the geometry of the aerofoil and physical behaviour of the fluid flow around it [8]. In fixed wing aerial vehicles, the flight

* Corresponding author.

E-mail addresses: hdkaraca@etu.edu.tr (H.D. Karaca), dozen@metu.edu.tr (G.D. Özen), coshku@gmail.com, kasnakoglu@etu.edu.tr (C. Kasnakoğlu).

depends on the lift force which increases along with propulsion; however, high propulsion brings higher drag force [9]. To obtain more efficient flight, it is needed to overcome this trade-off. Achieving enough lift force to practice flight with less propulsion and drag force is an active field of research. Efforts towards increasing lift include Lee et al. [10] who proposed a multi-disciplinary design methodology and achieved a significant lift enhancement using micro-scale devices for turbine blades; Bai et al. [11] who used a flow deflector which can suppress the flow separation, delay the stall, and enhance the lift; Colonus et al. [12] who developed a method to control of the angle of attack of an aerofoil to enhance lift force; and Shojaeferd et al. [13] who managed to increase the lift coefficient of an aerofoil with the help of blowing and suction. Enhancements through drag reduction have also received considerable research attention; studies in this direction include the work by Allan et al. [14] who used oscillatory flow excitation for the control of a generic model of an aerofoil, He et al. [15] who examined computational methods for active control and drag optimization of the incompressible viscous flow past cylinder, and Pastoor et al. [16] who investigated strategies for an elongated D-shaped body.

The goal of this study is to reduce the drag to lift ratio for aerofoils using active flow control based on nonlinear dynamical models obtained through system identification. A systematic methodology is developed and illustrated by case studies involving three commonly used aerofoils. This work complements the previous efforts of our research group on flow modelling [17,18], simulation [19,20] and control [21–23], while being unique in the sense that a systematic nonlinear modelling and control method for the flow around an aerofoil system based on unsteady incompressible flow data is developed and shown to yield successful results. The rest of this paper is organized as follows: Section 2 presents the problem description, Section 3 outlines the methodology, Section 4 discusses the results and Section 5 presents the conclusions.

2. Problem description

An aerofoil is the shape of an aircraft wing as seen in cross section. Fig. 1 shows the four main forces of flight acting on the aerofoil. The *weight* of the aircraft is directed downwards towards the earth. To achieve flight, the weight must be overcome by the *lift* force generated by the motion of the airplane through the air. The wing deflects the air downward and the opposite reaction pushes the wing up. The forward motion of the aircraft is attained by the *thrust* force generated by the engines. As the aerofoil pushes the air out of its way, the air pushes back on the aerofoil generating a *drag* force. This force is opposite to the motion direction and can be thought of as an aerodynamic friction. Wing structures are also used in boats, submarines and ships where the idea is similar but the fluid is water instead of air. When used in watercraft, these are often called *hydrofoils*.

The main goal of this study is to design a feedback control system to reduce the drag to lift (D/L) ratio (in other words to enhance the lift to drag (L/D) ratio) for flow over aerofoils using an actuator placed on the surface. To achieve this goal, a systematic method which consists of obtaining a nonlinear dynamical model by using system identification technique and designing a feedback controller system for the model is carried out for NACA 23012, ag13 and b737a aerofoils. The mesh structures constructed to be used for the computational fluid dynamics (CFD) simulations of these aerofoils are shown in Fig. 2, together with the points through which the actuators will be injecting or sucking fluid as necessary. The fluid flow is governed by the incompressible Navier–Stokes partial differential equations (PDEs)

$$\rho \left(\frac{\partial q}{\partial t} + (q \cdot \nabla) q \right) = -\nabla p + \mu \nabla^2 q$$

$$\nabla \cdot q = 0 \quad (1)$$

where $\rho \in \mathbb{R}_+$ is the density of the fluid, $\mu \in \mathbb{R}_+$ is the dynamic viscosity of the fluid, $p(x, y, t) \in \mathbb{R}$ is the pressure and $q(x, y, t) = (U(x, y, t), V(x, y, t)) \in \mathbb{R}^2$ is the flow velocity with u and v being the components in the streamwise and

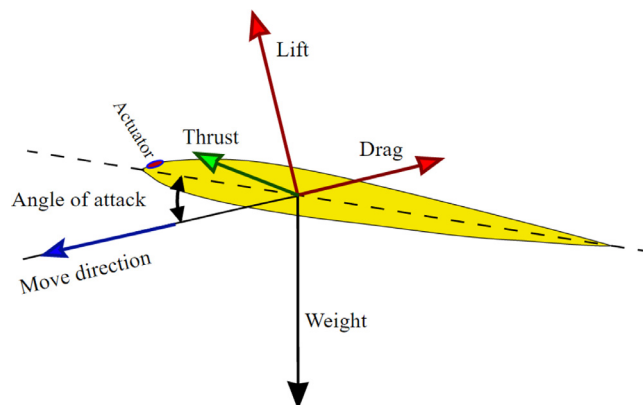


Fig. 1. Forces of flight on an aerofoil moving through a fluid [24]. The aim is to increase lift (L) and decrease drag (D), i.e. reduce the D/L ratio, using a small actuator placed on the surface.

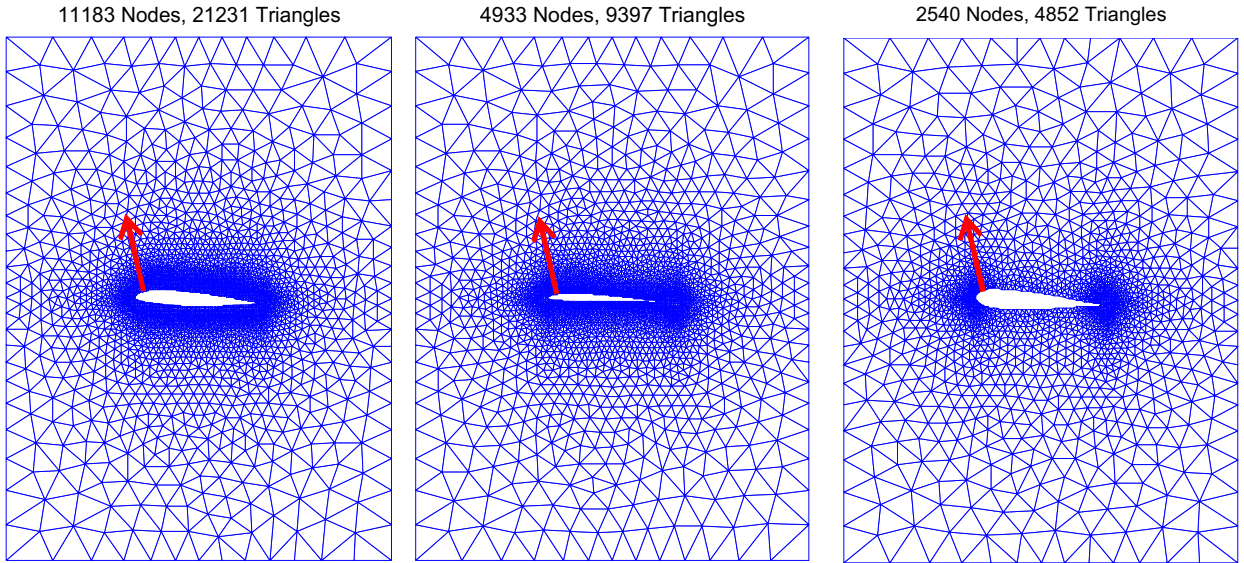


Fig. 2. The mesh used for CFD simulations of the NACA 23012 (left), ag13 (centre) and b737a (right) aerofoils. Also shown as the red arrow is the location and direction of actuation. (For interpretation of the references to colour in this figure legend, the reader is referred to the web version of this article.)

transverse directions. ∇ is the del operator denoting directional derivative $(q \cdot \nabla)q$, gradient ∇p , Laplacian $\nabla^2 q$ and divergence $\nabla \cdot q$ of the relevant flow variables. In two dimensions, Eq. (1) can be expanded as

$$\begin{aligned} \rho \left(\frac{\partial U}{\partial t} + U \frac{\partial U}{\partial x} + V \frac{\partial U}{\partial y} \right) &= -\frac{\partial p}{\partial x} + \mu \left(\frac{\partial^2 U}{\partial x^2} + \frac{\partial^2 U}{\partial y^2} \right) \\ \rho \left(\frac{\partial V}{\partial t} + U \frac{\partial V}{\partial x} + V \frac{\partial V}{\partial y} \right) &= -\frac{\partial p}{\partial y} + \mu \left(\frac{\partial^2 V}{\partial x^2} + \frac{\partial^2 V}{\partial y^2} \right) \\ \frac{\partial U}{\partial x} + \frac{\partial V}{\partial y} &= 0. \end{aligned} \quad (2)$$

The Navier–Stokes PDEs are solved using Navier2d, a CFD tool for MATLAB [25]. We have significantly modified and extended this program to accommodate our needs for the study in this paper; these modifications will be described in detail in the upcoming sections.

The boundary conditions and parameters used for the CFD simulations are as follows [26]: The flow domain is $\Omega = [-1 \text{ m}, 2 \text{ m}] \times [-2 \text{ m}, 2 \text{ m}]$, with an aerofoil whose leading edge is placed at the origin $(0, 0)$. The fluid is of density $\rho = 998.2 \text{ kg/m}^3$ and dynamic viscosity $\mu = 1.002 \times 10^{-3} \text{ kg/m} \cdot \text{s}$ and it flows into the flow domain from the left boundary at a velocity of 1 m/s, i.e. $U = 1 \text{ m/s}$ and $V = 0 \text{ m/s}$, where U and V denote the streamwise and transverse components of the flow velocity respectively. The top and bottom boundaries are assumed free-slip, i.e. $\frac{dU}{dn} = 0$ and $V = 0$ on these boundaries, where n is the normal direction to the boundary. The fluid is assumed to exit the flow domain at constant pressure from the right boundary. The aerofoils are assigned no-slip boundary conditions, i.e. $U = V = 0$ on the surface. Actuators placed on the upper surfaces of the aerofoils are capable of blowing or sucking fluid in a direction normal to the surface, as shown in Fig. 2. The sites of the actuators were determined empirically by performing numerous CFD simulations and selecting the locations where the lift and drag forces are affected the most.

3. Methodology

3.1. CFD simulations for generating input–output data

The first step is to perform CFD simulations of the flow using Navier2d to collect data to be used later in system identification. For this purpose we need to determine the input and output for the problem. For the actuation input we select a small number of nodes on the top surface of the aerofoils (Fig. 2) from where some fluid can be injected or sucked. Since our goal is to reduce the D/L value, we choose the lift and drag coefficients as measurements. Normally Navier2d does allow for defining such input output signals; hence we had to extend the program to include such a capability. We also implemented a data logger that records these input/output values at every time step of the simulation.

To excite the system sufficiently and reveal enough of the underlying dynamics, it is common practice in system identification to apply a signal that contains a variety of frequencies. For this purpose we use a chirp signal of unit magnitude and

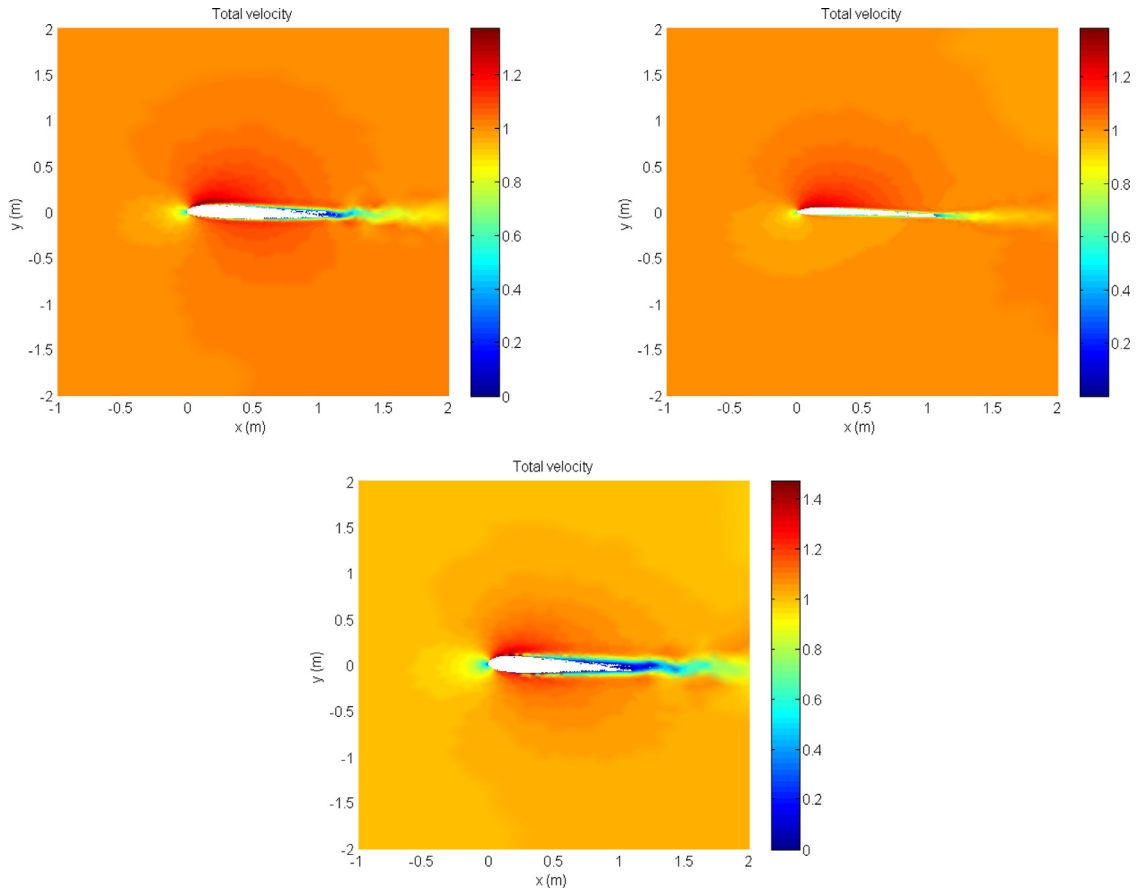


Fig. 3. CFD simulation snapshots for NACA 23012 (top left), ag13 (top right) and b373a (bottom) aerofoils.

duration of 50 s, where the frequency varies from 0.1 Hz to 1 Hz for the first 25 s and then goes from 1 Hz back to 0.1 Hz for the next 25 s. Selected snapshots from the CFD simulations of the NACA 23012, ag13 and b737a aerofoils are shown in Fig. 3. The figure only shows the total velocities as an example but a large set of data is generated and logged, which includes streamwise and transverse velocities, pressure, vorticity, forces acting of the aerofoils, lift and drag values and so on.

The input–output data resulting from CFD simulations for NACA 23012, ag13 and b737a aerofoils are shown in Figs. 4, 5 and 6 respectively. In the figures one can see that the input and output signals are partitioned into two parts, shown in different colours. The first 25 s of the data is the *estimation data* and will be used for building the dynamical model using system identification. The last 25 s of the data is the *validation data* which is not used in identification and is reserved for verifying the results of system identification.

The next step is to perform system identification on this input–output data to obtain the dynamical model of the flow process.

3.2. System identification for obtaining dynamical models

Once the input–output data is obtained we identify a Hammerstein–Wiener (HW) type nonlinear model to represent the flow behaviour. This modelling approach is based on the supposition that if the output of the system depends nonlinearly on its inputs, it is possible to decompose the input–output relation into two or more interconnected elements [27,28]. Substantial research has been devoted to the identification of HW models and controller design on systems represented by HW systems since these models can accurately represent many real-life engineering processes [29,30]. The Hammerstein–Wiener model consists of three serial blocks: an input nonlinearity f , a linear system block G and an output nonlinearity function h . The block diagram of a HW model is illustrated in Fig. 7. The input–output relationship of a HW model is denoted in operator notation as

$$y = h(G(f(u))). \quad (3)$$

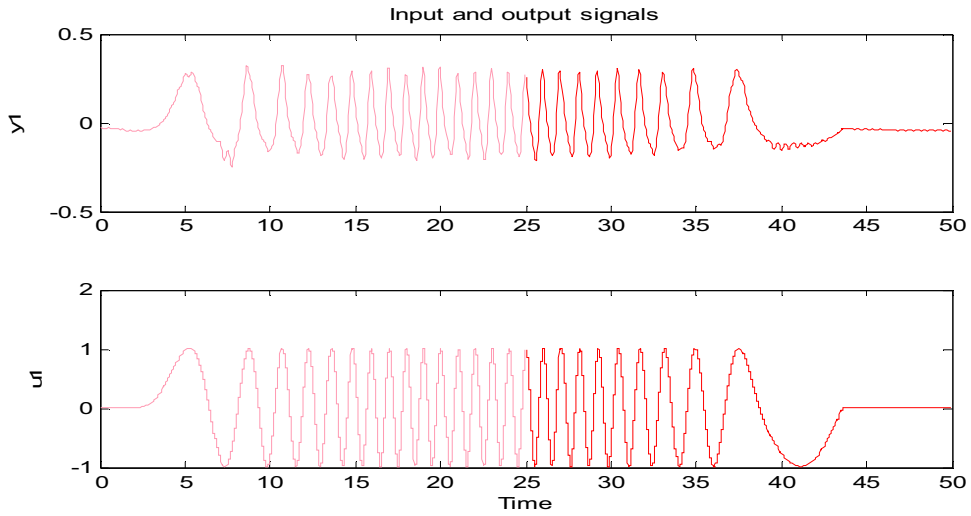


Fig. 4. Chirp signal input (u_1) and the resulting measured output (y_1) for NACA 23012 obtained from CFD simulations.

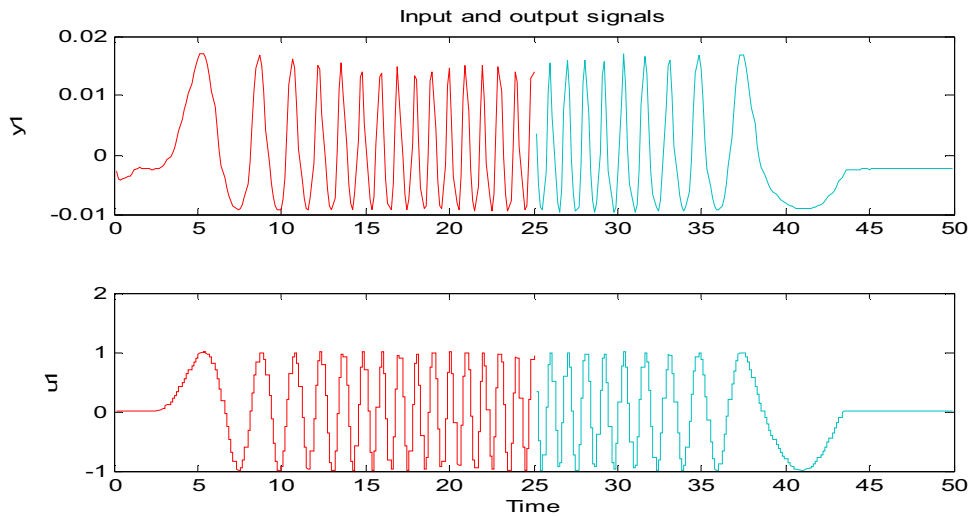


Fig. 5. Chirp signal input (u_1) and the resulting measured output (y_1) for ag13 obtained from CFD simulations.

While most system identification packages, including MATLAB System Identification Toolbox used in this study, are capable of building HW models with quite general input/output nonlinearity functions, the control of these models often becomes problematic or even impossible if the nonlinearities are of high degree and are noninvertible. We therefore impose additional restrictions on the identification process to benefit the controller design in the succeeding sections. The nonlinearities are constrained to be invertible polynomials of at most degree two on the domain of interest which is assumed to be $[-10, 10]$ for the input and $[0, 1]$ for the output, based on the physical properties of the system and CFD simulations. To elaborate, the input nonlinearity f is of the form

$$f(u) = \alpha_2 u^2 + \alpha_1 u + \alpha_0 \tag{4}$$

where $\alpha_2, \alpha_1, \alpha_0 \in \mathbb{R}$. The function has a single extremum point at $u = -\alpha_1/(2\alpha_2)$. To assure invertability in $[-10, 10]$, this point must lie outside the domain of interest, i.e.

$$-\frac{\alpha_1}{2\alpha_2} \leq -10 \quad -\frac{\alpha_1}{2\alpha_2} \geq 10. \tag{5}$$

Equivalently

$$\left| \frac{\alpha_1}{2\alpha_2} \right| \geq 10 \Leftrightarrow \frac{\alpha_1^2}{2^2 \alpha_2^2} \geq 10^2 \tag{6}$$

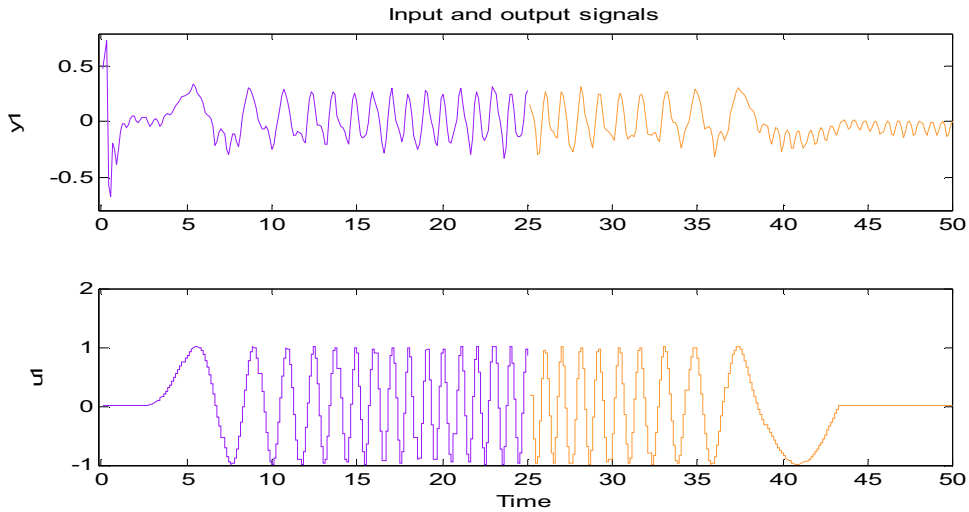


Fig. 6. Chirp signal input (u_1) and the resulting measured output (y_1) for b737a obtained from CFD simulations.

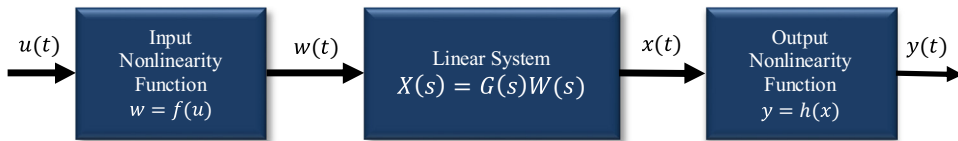


Fig. 7. Block diagram of Hammerstein–Wiener (HW) model.

which implies

$$\alpha_1^2 - 400\alpha_2^2 \geq 0. \tag{7}$$

Similarly the output nonlinearity h is of the form

$$h(x) = \beta_2x^2 + \beta_1x + \beta_0 \tag{8}$$

where $\beta_2, \beta_1, \beta_0 \in \mathbb{R}$. The function has a single extremum point at $x = -\beta/(2\beta_2)$. To assure invertability in $[0, 1]$, this point must lie outside the domain of interest, i.e.

$$-\frac{\beta_1}{2\beta_2} \leq 0 \quad -\frac{\beta_1}{2\beta_2} \geq 1 \tag{9}$$

Equivalently

$$\left| -\frac{\beta_1}{2\beta_2} - 0.5 \right| \geq 0.5 \Leftrightarrow \left(-\frac{\beta_1}{2\beta_2} - 0.5 \right)^2 \geq 0.5^2 \tag{10}$$

$$\frac{(-\beta_1 - \beta_2)^2}{2^2\beta_2^2} \geq 0.25 \Leftrightarrow (\beta_1 + \beta_2)^2 \geq \beta_2^2 \tag{11}$$

which implies

$$\beta_1^2 + 2\beta_1\beta_2 \geq 0. \tag{12}$$

For the linear part, a fourth order transfer function is utilized

$$G(s) = \frac{X(s)}{W(s)} = \frac{b_4s^4 + b_3s^3 + b_2s^2 + b_1s + b_0}{a_4s^4 + a_3s^3 + a_2s^2 + a_1s + a_0} \tag{13}$$

where $a_4, a_3, a_1, a_0, b_4, b_3, b_2, b_1, b_0 \in \mathbb{R}$. The cost function J to be minimized for estimation is defined as the integral squared error (ISE)

$$J(p) = \int_{t_{start}}^{t_{end}} e^2(\tau) d\tau \tag{14}$$

where

$$p = [a_4 \ a_3 \ a_2 \ a_1 \ a_0 \ b_4 \ b_3 \ b_2 \ b_1 \ b_0 \ \alpha_2 \ \alpha_1 \ \alpha_0 \ \beta_2 \ \beta_1 \ \beta_0]^T. \tag{15}$$

is the parameter vector, $[t_{start}, t_{end}] = [0, 25]$ is the estimation data interval,

$$e(t) = y_{data}(t) - y_{model}(t) \tag{16}$$

is the error between the estimation data (y_{data}) and the output of the HW model expressed as

$$y_{model} = h(G(f(u_{data}))).$$

The HW model estimation procedure can therefore be written as a nonlinear constrained optimization problem in standard form

$$\min_p J(p) \text{ s.t. } c_1(p) \geq 0 \text{ and } c_2(p) \geq 0 \tag{17}$$

where J is as in (14) and the inequality constraints are written from (7) and (12) as

$$c_1(p) = \alpha_1^2 - 400\alpha_2^2 \tag{18}$$

$$c_2(p) = \beta_1^2 + 2\beta_1\beta_2. \tag{19}$$

To solve the problem (17), a fast and efficient nonlinear programming method, namely Sequential Quadratic Programming (SQP), is employed [31,32]. For this purpose a Quadratic Programming (QP) subproblem based on a quadratic approximation of the Lagrangian function is formulated

$$\mathcal{L}(p, \sigma_1, \sigma_2) = J(p) - \sigma_1 c_1(p) - \sigma_2 c_2(p) \tag{20}$$

where σ_1 and σ_2 are Lagrange multipliers. At an iterate p_k , the SQP algorithm defines an appropriate search direction d_k as a solution to the QP subproblem

$$\min_d \frac{1}{2} d^T \nabla^2 \mathcal{L}(p_k, \sigma_{1,k}, \sigma_{2,k}) d + \nabla J(p_k)^T d \tag{21}$$

subject to

$$\nabla c_1(p_k)^T d + c_1(p_k) = 0, \quad \nabla c_2(p_k)^T d + c_2(p_k) = 0. \tag{22}$$

The subproblem is in standard QP form hence it can be tackled with any QP algorithm readily available in many numerical solver packages [33]. The solution d_k to this problem is utilized to form a new iterate

$$p_{k+1} = p_k + \alpha_k d_k \tag{23}$$

where the step length α_k is obtained by an appropriate line search procedure so that an adequate decrease in the following merit function is obtained

$$\Psi(p) = J(p) + r_1 c_1(p) + r_2 c_2(p). \tag{24}$$

The penalty parameters r_1 and r_2 are positive constants.

Using the procedure described above, the input nonlinearity function obtained from system identification for NACA 23012 is

$$y = -0.0314 x^2 + 0.9650 x - 0.0385 \tag{25}$$

and the output nonlinearity function is

$$y = 0.0162 x^2 + 0.0928 x - 0.0337. \tag{26}$$

The input and output nonlinearity functions for ag13 aerofoil are respectively

$$y = 0.0368 x^2 + 1.0144 x - 0.0048 \tag{27}$$

$$y = 0.0615 x^2 + 0.0429 x - 0.0018. \tag{28}$$

The input and output nonlinearity functions for ag13 aerofoil are respectively

$$y = x \tag{29}$$

$$y = x. \tag{30}$$

The last two equations denote simply that the best Hammerstein–Wiener model for the flow over b737a aerofoil is indeed a purely linear one. These nonlinearity functions given above are plotted in Figs. 8–10 from where one can also confirm that they are invertible on the domains of interest.

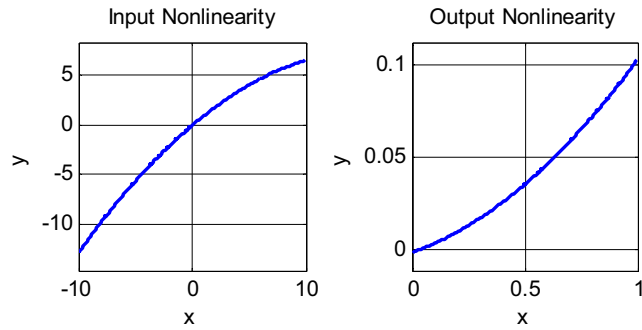


Fig. 8. Input and output nonlinearity functions for the Hammerstein–Wiener (HW) model of the NACA 23012 aerofoil.

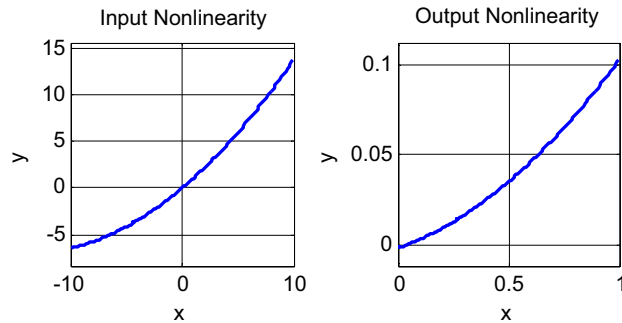


Fig. 9. Input and output nonlinearity functions for the Hammerstein–Wiener (HW) model of the ag13 aerofoil.

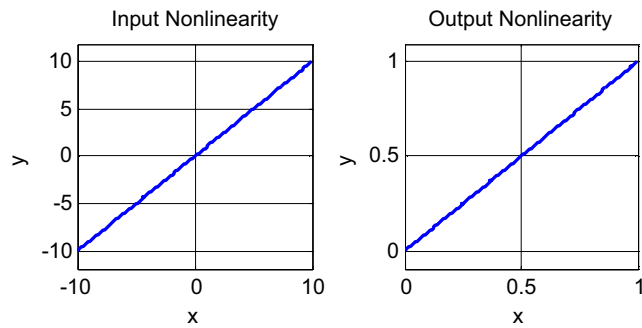


Fig. 10. Input and output nonlinearity functions for the Hammerstein–Wiener (HW) model of the b737a aerofoil.

The identified linear blocks of the HW models for NACA 23012, ag13 and b737a aerofoils are listed below respectively.

$$G(s) = \frac{9.419 s^2 + 355 s + 1532}{s^3 + 4.779 s^2 + 164s + 613.4} \quad (31)$$

$$G(s) = \frac{11.58 s^3 + 170.2 s^2 + 5988 s + 3.271 \cdot 10^4}{s^4 + 1.429 s^3 + 782.4 s^2 + 596.1 s + 1.397 \cdot 10^5} \quad (32)$$

$$G(s) = \frac{2.689 s^2 + 39.57 s + 28.89}{s^3 + 5.838 s^2 + 197.7 s + 191.3} \quad (33)$$

Finally Figs. 11–13 show the full range of the measured data obtained from CFD simulations (denoted as *measured output*) compared to the simulated output produced by the HW models (denoted as *simulated output*). It can be observed from the figures that the Hammerstein–Wiener model adequately captures the general trend of the flow process in terms of predicting the effect of actuation on the D/L ratio. There are certainly some deviations and regions of mismatch, but this is to be expected since a perfect match between a simple low-order dynamical ordinary differential equation (ODE) model and the complicated infinite order Navier–Stokes (NS) partial differential equations (PDEs) would be unrealistic.

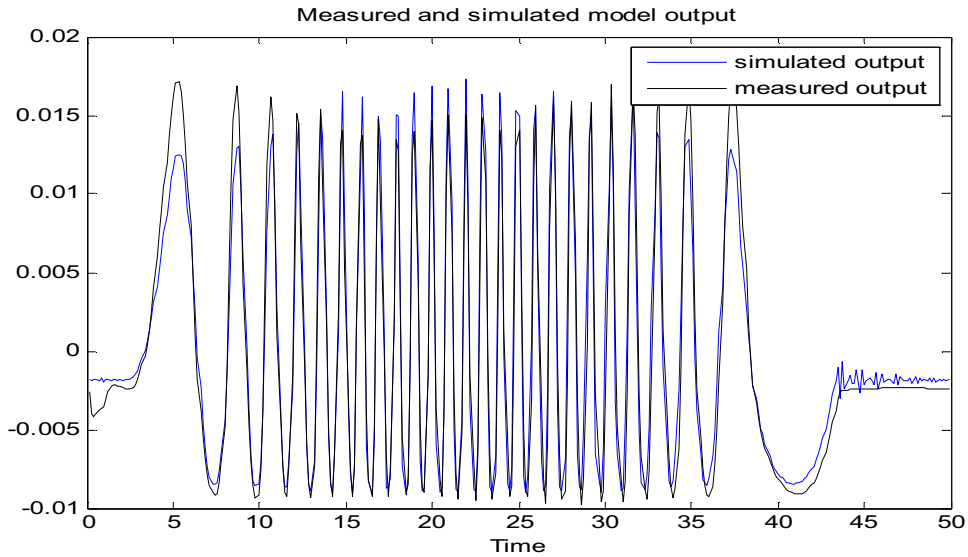


Fig. 11. Simulated and measured outputs for NACA 23012.

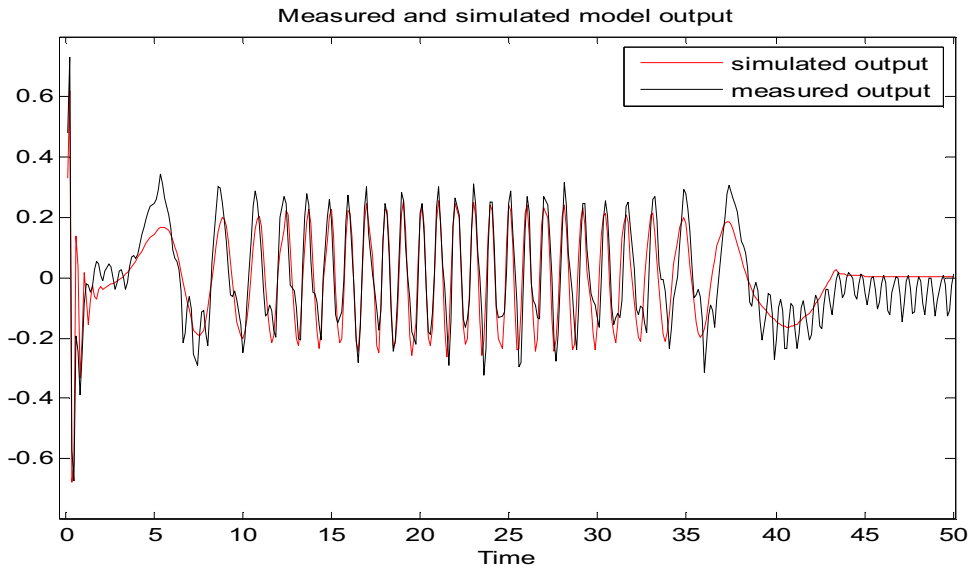


Fig. 12. Simulated and measured outputs for ag13.

3.3. Controller design

The next step is to design controllers for the nonlinear Hammerstein–Wiener models obtained in the previous section to regulate the system output, i.e. the drag to lift (D/L) ratio. Because the input and output nonlinearity functions are constructed to be invertible, the controller design can first be carried out on the linear part using standard linear control theoretic approaches, and then the inputs and outputs can be mapped bijectively to the nonlinear HW model [34]. Numerous standard and automated design methods exist for obtaining the controller $C(s)$ on the linear part of the model such as Ziegler–Nichols PID tuning technique, internal model control (IMC), linear quadratic Gaussian (LQG) synthesis and optimization-based approaches. For the current problem, various compensators of different orders were constructed and tested using these methods with the help of MATLAB Control Systems Toolbox. The best results were obtained using Ziegler–Nichols PID tuning method [35] which resulted in the controllers

$$C(s) = \frac{0.0011654 (s + 34.42)}{s} \tag{34}$$

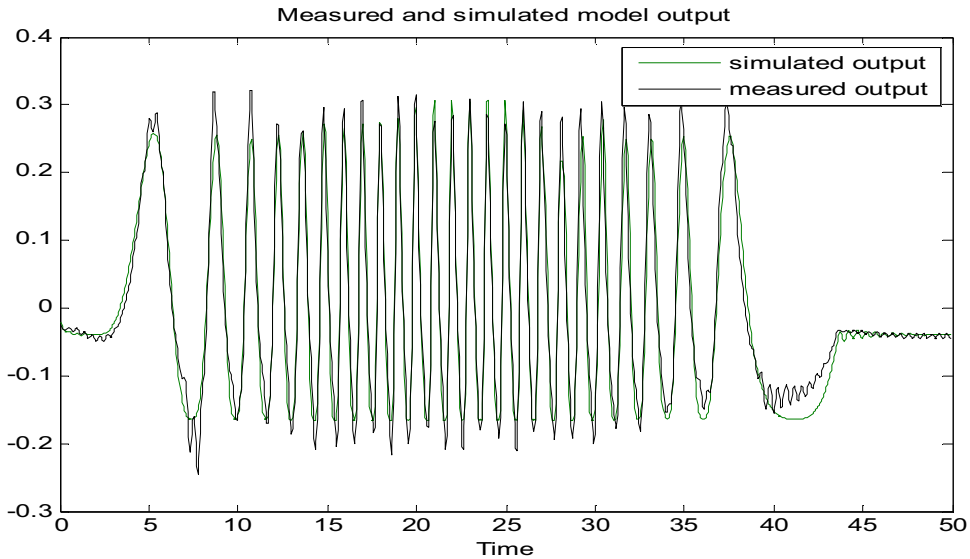


Fig. 13. Simulated and measured outputs for b737a.

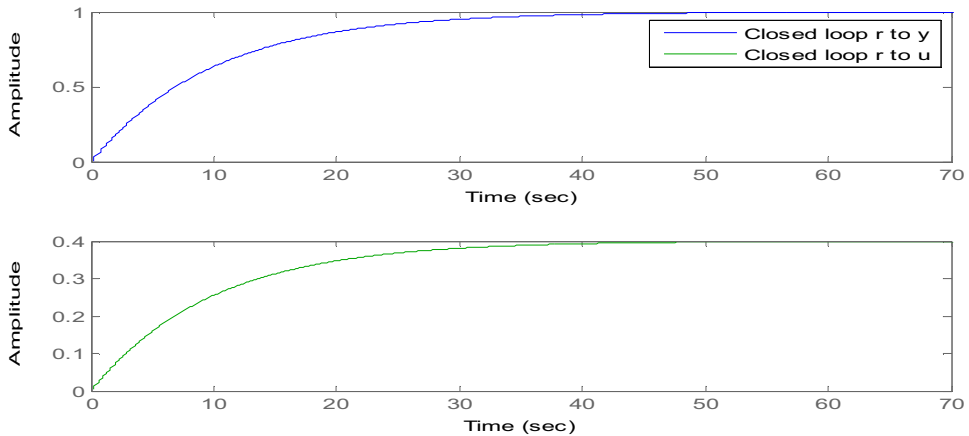


Fig. 14. Step response (top) and control effort (bottom) for NACA 23012.

for the NACA 23012 aerofoil,

$$C(s) = \frac{0.084738 (s + 14.31)}{s} \quad (35)$$

for the ag13airfoil, and

$$C(s) = \frac{0.085442 (s + 16.44)}{s} \quad (36)$$

for the b737a aerofoil. The closed-loop step responses and controller efforts for the linear blocks are shown in Figs. 14–16. It can be observed that the controllers successfully achieve the desired tracking with reasonable speed and damping characteristics while keeping the control effort within workable limits.

3.4. Integrating the controller to the simulation

In order to achieve closed-loop simulations, the controllers designed need to be integrated into the Navier2d CFD solver. This integration is carried out by embedding the controller designed into Simulink, which is the block simulation environment of MATLAB. The Simulink model also carries out the inversion of the nonlinearity functions of the HW model and the interfacing with Navier2d, as shown in Fig. 17.

During every simulation step, the Simulink model gathers the measured output computed by the CFD solver Navier2D (denoted *measureNow*) and passes this value through the inverse output nonlinearity block to the output of the linear model

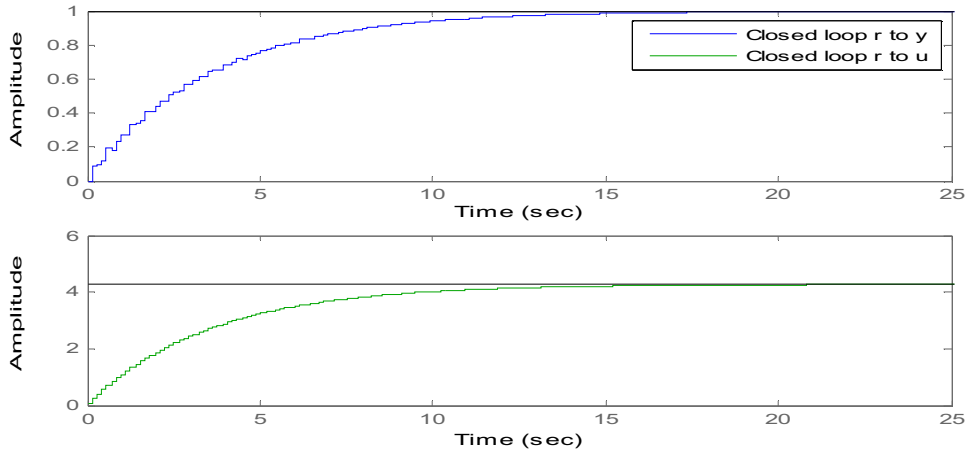


Fig. 15. Step response (top) and control effort (bottom) for ag13.

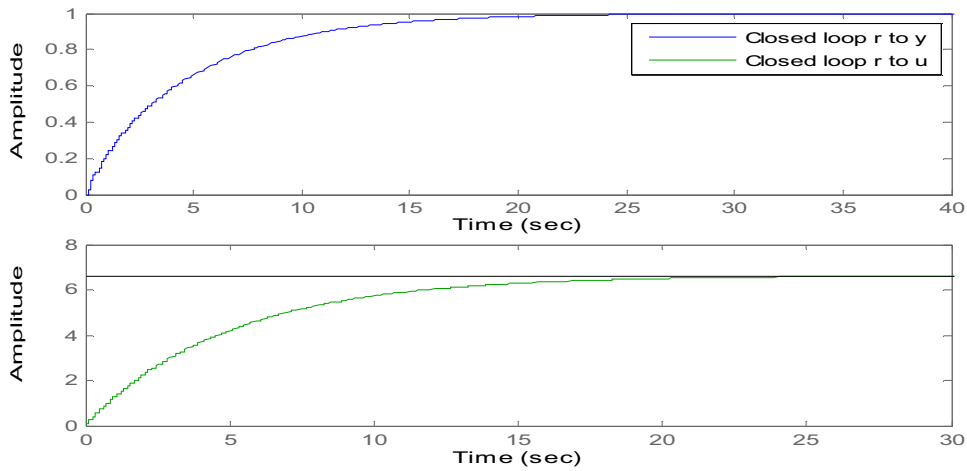


Fig. 16. Step response (top) and control effort (bottom) for b737a.

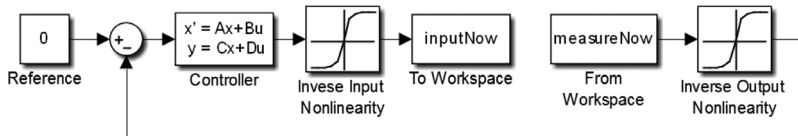


Fig. 17. Simulink block diagram for carrying out the closed loop simulations.

corresponding to this measured value. This value is then compared with the desired output value to obtain the error; the desired value is typically set to zero since the goal is to make the D/L value as small as possible. This error is then fed to the controller, which produces the input signal that needs to be applied to the linear block of the model. This value is then mapped to the input of the nonlinear HW model through the inverse input nonlinearity block. The result is the value of actuation to be applied to the flow process, which is then sent to the CFD solver through a workspace variable (denoted *inputNow*). These steps are repeated for every iteration of the CFD simulation.

4. Results

To test the modelling and control approach, closed-loop CFD simulations were run for the NACA 23012, ag13, and b737a geometries. The simulations are run unactuated without the controller until the transients decay and the flow settles, after which the controller is switched on. The first result, which is D/L vs. time for NACA 23012, can be investigated in Fig. 18. Until $t = 250$ s, the simulation is performed under no control in order to observe the D/L ratio in steady state. At $t = 250$ s, the feedback controller switches on. The reduction of D/L value can be observed from the figure. A similar closed-loop simulation is carried out for the ag13 and b737a aerofoils, and the result is shown in Figs. 19 and 20 respectively. One can again observe that the D/L ratio is reduced significantly.

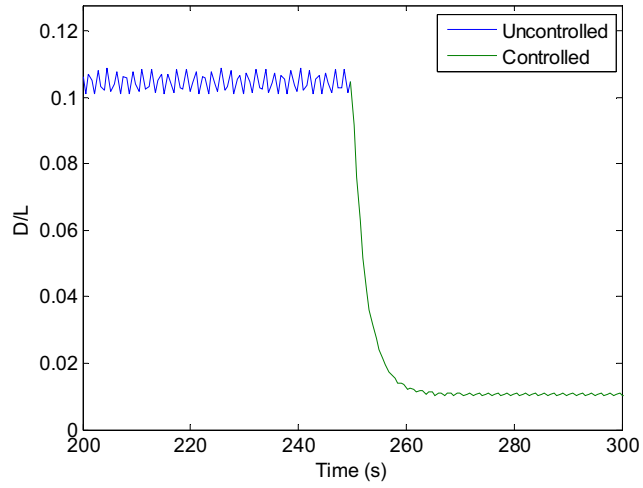


Fig. 18. Closed-loop simulation results for NACA 23012. Controller is switched on at $t = 250s$.

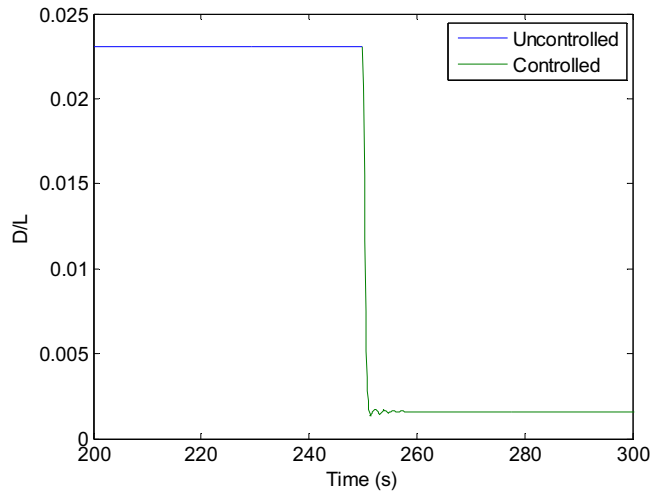


Fig. 19. Closed-loop simulation results for ag13. Controller is switched on at $t = 250s$.

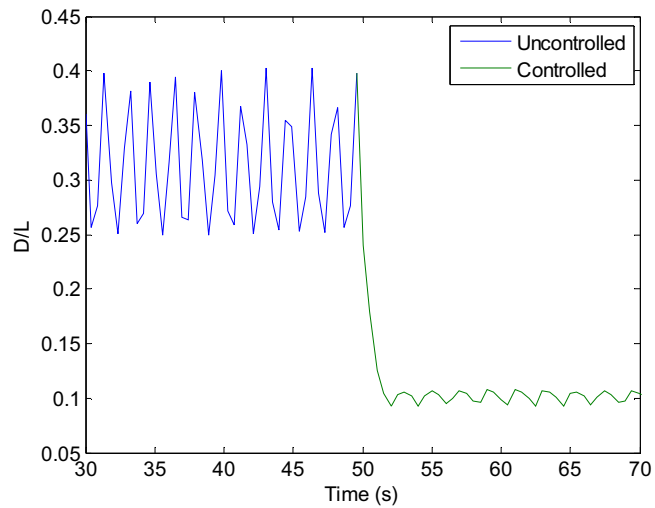


Fig. 20. Closed-loop simulation results for b737a. Controller is switched on at $t = 50s$.

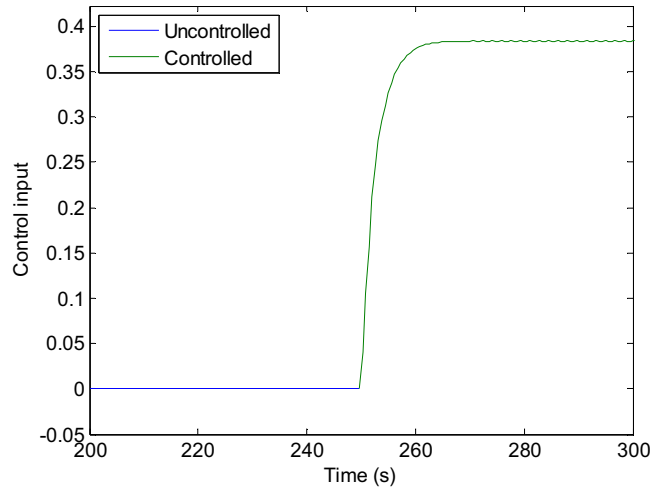


Fig. 21. Closed-loop control effort for NACA 23012. Controller is switched on at $t = 250$ s.

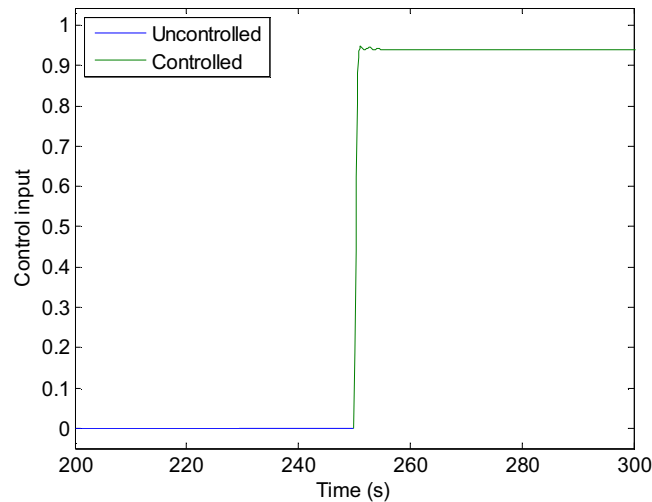


Fig. 22. Closed-loop control effort for ag13. Controller is switched on at $t = 250$ s.

It may be remarked for all cases that although the reference values to the closed-loop system are set to zero, it can be seen from the figures that the D/L ratio never reaches zero as this would imply zero drag and/or infinite lift, which is practically impossible. Providing zero to the reference value simply instructs the closed-loop system to render the output value as small as possible.

As an additional analysis, the control input levels for the NACA 23012, ag13 and b737a aerofoils are provided in Figs. 21, 22 and 23 respectively. It can be seen from the figures that the control input values are of the same order of magnitude with the mean flow and do not exceed unit value, which strengthens the physical meaningfulness of the procedure.

5. Conclusions and future works

In this study the nonlinear modelling and feedback control of the drag to lift (D/L) ratio for three aerofoils was studied. Input–output data collected by means of computational fluid dynamics (CFD) simulations was used in system identification to construct a Hammerstein–Wiener type nonlinear model for the flow process. A special restriction was imposed during identification so that the input–output nonlinearity functions of the HW model are designed to be invertible over the domain of interest. This property was exploited during control design by first designing controllers for the linear block of the HW model, and then mapping the inputs and outputs to the nonlinear model through the inverse functions of the nonlinearities. CFD simulations for the closed-loop system demonstrated that the controller efficiently suppresses D/L ratio to a significant fraction of the uncontrolled scenario.

In light of the promising results obtained in this paper, our future works include applying the proposed method to a broader range of aerofoils from turbulent, laminar and natural laminar families, as well as experimenting with different

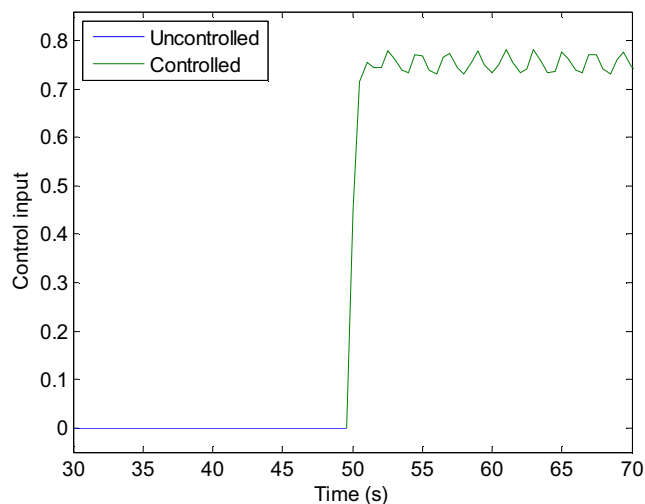


Fig. 23. Closed-loop control effort for b737a. Controller is switched on at $t = 50$ s.

speed regimes, varying angle of attack and compressible flows. We also plan on testing the proposed technique on an actual experimental setup and comparing the results with those obtained in this paper.

Acknowledgments

This work was supported by the Scientific and Technological Research Council of Turkey (TUBITAK) under projects 109E233, 113E581 and by the European Commission (EC) under project PIRG-2008-GA-239536.

References

- [1] C.W. Rowley, T. Colonius, R.M. Murray, Model reduction for compressible flows using POD and Galerkin Projection, *Physica D: Nonlinear Phenom.* 189 (1) (2004) 115–129.
- [2] G.M.R. van Raemdonck, P. van Leeuwen, M.J.L. van Tooren, Comparison of experimental and numerically obtained flow properties of a bluff body, *The Aerodynamics of Heavy Vehicles III*, Springer International Publishing, 2016, pp. 393–411.
- [3] H. Jouharaa, B.P. Axcell, Modelling and simulation techniques for forced convection heat transfer in heat sinks with rectangular fins, *Simul. Modell. Pract. Theory* 17 (5) (2009) 871–882.
- [4] E. Shaik, K.A. Hoffmann, J.F. Dietiker, Numerical simulations of pulsatile non-Newtonian flow in an end-to-side anastomosis model, *Simul. Modell. Pract. Theory* 16 (9) (2008) 1123–1135.
- [5] M. Gad-el-Hak, *Flow Control: Passive, Active, and Reactive Flow Management*, Cambridge University Press, New York, 2000.
- [6] H. Liang, S. Cao, S. Zhang, J. Bai, Experimental investigation of airfoil suction side flow separation control by spanwise nanosecond actuation, *Measuring Technol. Mechatron. Autom.* 2 (2011) 108–111.
- [7] D. Greenblatt, I.J. Wygnanski, The control of flow separation by periodic excitation, *Prog. Aerosp. Sci.* 36 (7) (2000) 487–545.
- [8] C. Rethmel, J. Little, K. Takashima, A. Sinha, I. Adamovich, M. Samimy, Flow separation control over an airfoil with nanosecond pulse driven DBD plasma actuators, in: *AIAA Aerospace Sciences Meeting including the New Horizons Forum and Aerospace Exposition*, Orlando, Florida, 2011.
- [9] D. Raymer, *Aircraft Design: A Conceptual Approach*, AIAA Education Series, AIAA, Washington, 2002.
- [10] C. Lee, G. Hong, Q.P. Ha, S.G. Mallinson, A piezoelectrically actuated micro synthetic jet for active flow control, *Sens. Actuators A: Phys.* 108 (1) (2003) 168–174.
- [11] Y. Bai, X. Ma, X. Ming, Lift enhancement of aerofoil and tip flow control for wind turbine, *Appl. Math. Mech.* 32 (7) (2011) 825–836.
- [12] T. Colonius, C.W. Rowley, G. Tadmor, D.R. Williams, K. Taira, W.B. Dickson, M. Gharib, M. Dickinson, Closed-loop control of leading-edge and tip vortices for small UAV, in: *First Berlin Conference on Active Flow Control*, Berlin, Germany, 2006.
- [13] M.H. Shojaeifard, A.R. Noorpoor, A. Avanesians, M. Ghaffarpour, Numerical investigation of flow control by suction and injection on a subsonic airfoil, *Am. J. Appl. Sci.* 2 (10) (2005) 1474–1480.
- [14] B. Allan, J.-N. Juang, D. Raney, A. Seifert, L. Pack, D. Brown, Closed loop separation control using oscillatory flow excitation, *ICASE Report*, no. 2000-32, 2000.
- [15] J.W. He, R. Glowinski, R. Metcalfe, A. Nordlander, J. Periaux, Active control and drag optimization for flow past a circular cylinder, *J. Comput. Phys.* 163 (1) (2000) 83–117.
- [16] M. Pastoor, L. Henning, B.R. Noack, R. King, G. Tadmor, Feedback shear layer control for bluff body drag reduction, *Journal of Fluid Mechanics* 608 (2008) 161–196.
- [17] T.N. Erbil, C. Kasnakoglu, Feedback flow control employing local dynamical modelling with wavelets, *Math. Comput. Modell. Dyn. Syst.* 15 (6) (2009) 493–513.
- [18] C. Kasnakoglu, R.C. Camphouse, A. Serrani, Reduced-order model-based feedback control of flow over an obstacle using centre manifold methods, *J. Dyn. Syst. Meas. Control* 131 (1) (2009) 011011.
- [19] A. Paksoy, B. Apacoglu, S. Aradag, C. Kasnakoglu, Analysis of flow over a circular cylinder by CFD and reduced order modelling, in: *ASME 2010 10th Biennial Conference on Engineering Systems Design and Analysis*, 2010, pp. 377–384.
- [20] C. Kasnakoglu, M. Ö. Efe, Prediction of dynamical properties of flow over a three-element aerofoil via computationally intelligent architectures, in: *International Conference on Control, Automation and Systems (ICCAS 2008)*, 2008, pp. 381–386.
- [21] C. Kasnakoglu, A. Serrani, Analysis and nonlinear control of Galerkin models using averaging and centre manifold theory, in: *American Control Conference (ACC'07)*, 2007, pp. 3035–3040.
- [22] C. Kasnakoglu, Control of nonlinear systems represented by Galerkin models using adaptation-based linear parameter-varying models, *Int. J. Control Autom. Syst.* 8 (4) (2010) 748–761.

- [23] C. Kasnaçoğlu, Control of oscillations in flow problems under frequency limitations, *J. Vib. Control* 16 (13) (2010) 1941–1966.
- [24] B. Kosiorek, Forces on an aircraft wing, licensed CC BY-SA 3.0, <https://commons.wikimedia.org/w/index.php?curid=529226>, 2016 (accessed on 14.06.16).
- [25] D. Engwirda, An unstructured mesh Navier-Stokes solver (Master's thesis). School of Engineering, University of Sydney, 2005.
- [26] H.D. Karaca, Linear and nonlinear dynamic modeling and control of various fluid flow problems, (Master's thesis). Department of Electrical and Electronics Eng., TOBB University of Economics and Technology, 2012.
- [27] P. Crama, J. Schoukens, Hammerstein-Wiener system estimator initialization, *Automatica* 40 (9) (2004) 1543–1550.
- [28] E.W. Bai, A blind approach to the Hammerstein-Wiener model identification, *Automatica* 38 (6) (2002) 967–979.
- [29] B. Ding, X. Ping, Dynamic output feedback model predictive control for nonlinear systems represented by Hammerstein-Wiener model, *J. Process Control* 22 (9) (2012) 1773–1784.
- [30] F. Yu, Z. Mao, M. Jia, Recursive identification for Hammerstein-Wiener systems with dead-zone input nonlinearity, *J. Process Control* 23 (8) (2013) 1108–1115.
- [31] R. Fletcher, *Practical Methods of Optimization*, John Wiley and Sons, New York, 1987.
- [32] K. Schittkowski, NLPQL: a FORTRAN subroutine solving constrained nonlinear programming problems, *Ann. Oper. Res.* 5 (2) (1986) 485–500.
- [33] P.E. Gill, W. Murray, M.A. Saunders, M.H. Wright, Procedures for optimization problems with a mixture of bounds and general linear constraints, *ACM Trans. Math. Software (TOMS)* 10 (3) (1984) 282–298.
- [34] H.D. Karaca, G.D. Özen, C. Kasnaçoğlu, A nonlinear dynamical modeling and control method for the vorticity control of the flow past a circular cylinder, *Int. J. Mater. Mech. Manuf.* 1 (4) (2013) 324–346.
- [35] K.J. Åström, T. Hägglund, Revisiting the Ziegler-Nichols step response method for PID control, *J. Process Control* 14 (6) (2004) 635–650.